ADVANCED OPTICAL MATERIALS
www.advopticalmat.de

GaN Ultraviolet Laser based on Bound States in the Continuum (BIC)

Mu-Hsin Chen, Di Xing, Vin-Cent Su, Yang-Chun Lee, Ya-Lun Ho, and Jean-Jacques Delaunay**

Optical bound states in the continuum (BICs), realizing substantial suppression of out-of-plane radiative losses, have been utilized to realize strong light confinement and optical modes with high quality-factor (*Q*). Lasing actions with narrow linewidths based on optical BIC modes have been demonstrated in the near-infrared and the visible ranges, but BIC-based lasers in the ultraviolet (UV) region have not been reported. As light sources possessing wavelengths at the UV scale are essential in various fields, the strategy to design compact UV lasers based on high-*Q* modes and directional emissions is highly desirable. Here, the first BIC-based laser in the UV region is demonstrated by designing a 1D periodic resist structure on top of a GaN film. Using the symmetric-protected BIC mode, the fabricated laser is having a directional single-mode lasing emission with a small full-width at half-maximum of 0.10 nm and beam divergence of 1.5°. The lasing action is observed with a periodic structure area corresponding to a structure side length as small as 8 µm. Moreover, the wavelength control of the UV lasing is achieved by varying the period and temperature. This work provides strategies to design UV lasers having a small footprint together with narrow-linewidth and out-of-plane emissions.

1. Introduction

Cavities provide spatiotemporal confinement of energy that facilitates light-matter interactions and play an important role in optical physics. In recent years, a new type of optical mode realizing light confinement named optical bound states in the continuum (BICs) has been reported.[1] The effect was first observed from a surface-emitting distributed feedback laser.[2,3] In these BIC states, light is in completely localized states within the continuous spectrum of the environment with out-of-plane radiative losses completely suppressed.[1,4,5] Therefore, BICs are recognized to be a potential tool for light confinement and dramatic enhancement of the quality factor (*Q*) in periodic structures. The optical BIC states in a wave system have been widely discussed and utilized. The quasi-BIC effect was first reported in passive systems in the form of a 1D line-and-space periodic structure.[6] Subsequently, some passive devices utilizing BIC modes supported in metallic metasurfaces,[7,8] dielectric metasurfaces,[9–11] and photonic elements[12,13] are demonstrated. In an active device, a BIC mode can support narrow-linewidth lasing with a smaller device size down to a few dozen periods of the BIC structure, which makes it possible for the laser device to be integrated at high density onto a chip.[14] Due to these advantages of BIC in light confinement, BIC-supported lasers in the NIR range were realized.[14–17] The lasing emission is observed from a nanoarray structure having feature sizes smaller than 10 µm. Later, BIC-supported lasers were realized in the visible range.[18–24] A high-speed optical switch with vortex lasing emission is also realized via BICs in the visible range. However, a BIC-supported nanolaser emitting in the ultraviolet (UV) has not yet been reported.

With wavelengths ranging from 200 to 400 nm, UV nanolasers hold important applications in high-resolution bioimaging, laser therapy, spectroscopy, lithography, and optical storage. GaN with a wide direct bandgap of 3.41 eV at room temperature is the technological material employed for UV laser diodes. With the advanced of growth techniques such as metal-organic chemical vapor deposition (MOCVD) and vapor phase epitaxy growth method,[25,26] high-quality GaN can be readily deposited so that GaN-based UV lasers have been realized using single-crystal GaN film,[27,28] Fabry–Perot nanowire cavities,[29–33] whispering-gallery-mode cavities,[34–38] and vertical cavity surface emitting lasers (VCSEL).[39,40] For random scattering lasers, Fabry-Perot lasers, and whispering-gallery-mode lasers, out-of-plane directional emission lasing remains difficult to achieve. In contrast, VCSELs are designed for out-of-plane emission but require a relatively large cavity to support lasing action. BIC-based lasers have the potential to realize highly directional emissions with small device sizes.

Here, we demonstrate a BIC-based UV laser with directional emission and tunable emission wavelength that is fabricated on a standard GaN thin film without any etching step. A 1D periodic resist structure supporting the BIC mode was fabricated directly on the GaN thin film by a single-step electron-beam (e-beam)

M.-H. Chen, D. Xing, Y.-C. Lee, Y.-L. Ho, J.-J. Delaunay
School of Engineering
The University of Tokyo
7-3-1 Hongo, Bunkyo-ku, Tokyo 113–8656, Japan
E-mail: ho.ya-lun@scale.t.u-tokyo.ac.jp; jean@mech.t.u-tokyo.ac.jp
V.-C. Su
Department of Electrical Engineering
National United University
Miaoli 36003, Taiwan
The ORCID identification number(s) for the author(s) of this article can be found under https://doi.org/10.1002/adom.202201906.

DOI: 10.1002/adom.202201906

lithography process. Due to the strong light confinement of the BIC mode, the lasing action was observed at a finite device size of 8 μm. In addition, a narrow linewidth with full-width at half-maximum (FWHM) of 0.10 nm was observed which is among the smallest in the reported GaN-based single-mode UV lasers. We also demonstrated lasing up to a high temperature of 383 K showing potential for practical applications under relatively high-temperature environments. The lasing also showed a highly directional emission with a beam divergence of 1.5°. Furthermore, by adjusting the structure period and operating temperature, the control of the emission wavelength in a step of 0.45 nm over a wide range was achieved. It is noted that single-mode UV lasers with good monochromaticity and accurate wavelength control are highly desired for practical applications including photochemical, analytical, and spectroscopic.[41] Furthermore, since GaN has been widely utilized in semiconductor and optoelectronic devices as important technical semiconductor materials, the demonstration of GaN-based UV lasers supporting BIC modes may pave the way for electric-driven BIC lasers[42] in the UV region and expand their practical applicability.

2. Results and Discussion

2.1. Design

The schematic of the designed GaN UV BIC-based laser (referred to as "GaN BIC laser" in the following) is shown in **Figure 1**a. The GaN BIC laser is composed of a 1D e-beam resist line-and-space periodic structure, which supports the BIC mode, on a GaN film, as the gain medium. It should be emphasized that the proposed GaN BIC laser is fabricated by a single-step e-beam lithography process.

The primary parameter of the structure supporting the BIC mode, the period of the structure, was first investigated. To determine the period of the line-and-space periodic structure, the reflectance spectrum as a function of the incident wavelength and lattice period was calculated (Figure S1, Supporting Information). The thickness of GaN film was initially fixed at 800 nm, which is the original thickness of the prepared sample. The incident light is TE polarized as defined in Figure S1a (Supporting Information), and the fill factor was fixed at 0.5. As the structure period increases from 150 to 300 nm, resonance modes of different orders show up in the calculated reflectance mapping. It is noted that Q of the resonance mode decreases as the period increases, indicating that large periods cannot confine energy with a high-Q resonance. On the other hand, as line-and-space structures with small periods are impractical from the aspect of fabrication, the period should not be too small in the real design. In this study, we investigate the period of 200 nm unless specified otherwise.

To gain some insights into the resonances of the proposed line-and-space periodic structure, the reflectance spectrum around the emission band edge of GaN was calculated (Figure 1b). The reflectance spectrum reveals two resonance bands gradually separating as the angle of incidence ϕ increases. The mode at normal incidence on the upper band is referred to as the diffraction-coupled band-edge mode, or the

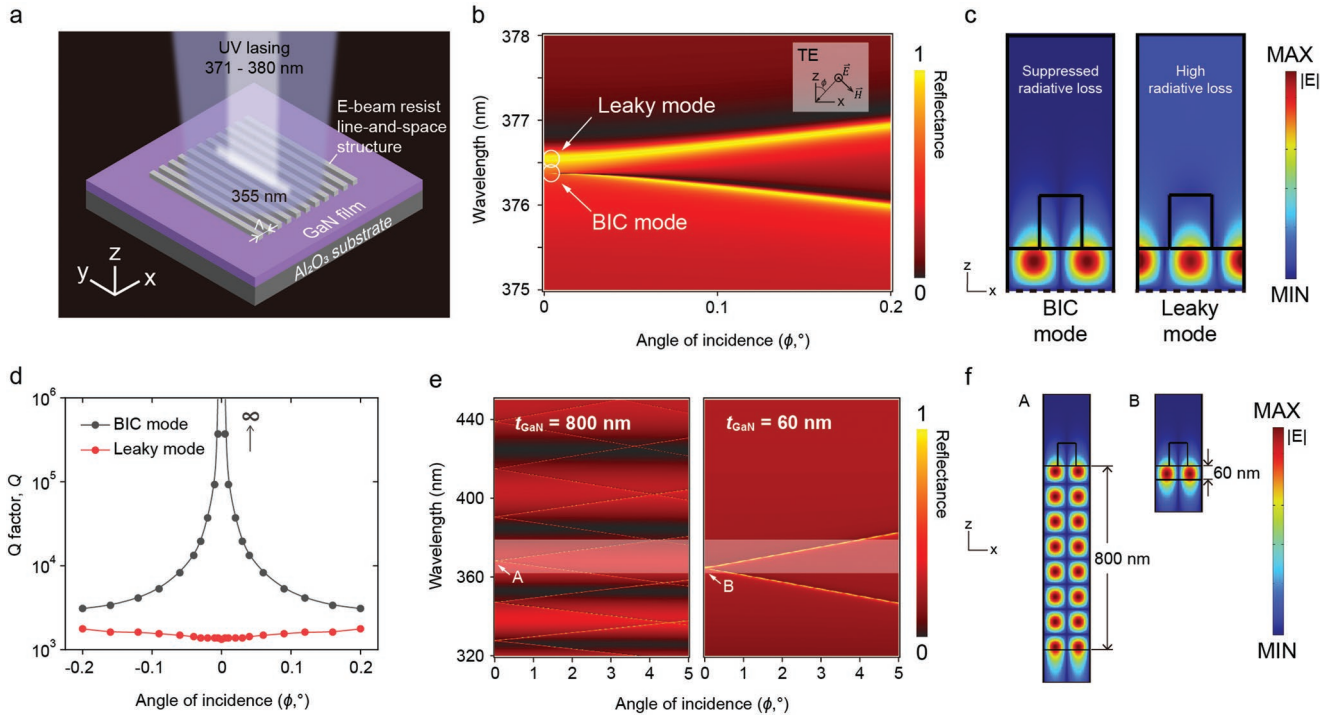

Figure 1. Ultraviolet (UV) laser based on bound-states-in-the-continuum (BIC). a) The schematic of the GaN UV BIC-based laser, which is composed of a 1D patterned electron-beam resist periodic structure supporting the BIC mode on a GaN film. b) Simulated reflectance spectra of the periodic structure for TE-polarized incident light, as defined in the inset. c) Simulated electric field norm distributions of the BIC mode and the leaky mode. d) Dependence of Q-factors (Q) of BIC modes and leaky modes on the angle of incidence. e) Wide-range reflectance spectra with different GaN thicknesses (t_{GaN}). f) Simulated electric field norm distributions of BIC modes for GaN thicknesses of 800 and 60 nm.

leaky mode, in which light can couple with the outgoing field and radiate.[22,43] In contrast, the BIC mode with typical dark-mode features is found at normal incidence on the lower band with a shorter wavelength.[20] The dispersion diagram for the structure is calculated and shown in Figure S2b (Supporting Information). The parabolic region near the high symmetric point (Γ point) reveals a group velocity of zero in the lateral (*x*-) direction, which is critical in providing optical feedback for lasing. The calculated near-field electric field distributions of these two modes are shown in Figure 1c. The leaky mode exhibits strong radiative losses to the far field while the radiative losses for the BIC mode are highly suppressed. This results in significant differences in the calculated *Q* between the two modes, as seen in Figure 1d. The leaky mode is observed to have a low *Q* of around 10^3 and a weak dependence of *Q* on the incidence angle, whereas the *Q* of the BIC mode is observed to grow rapidly and diverge toward infinity as the incidence angle approaches zero.

The effect of the GaN film thickness was also investigated through simulations. The reflectance spectrum of the periodic structure with an 800 nm GaN thickness (t_{GaN}) was calculated for a wide range of wavelengths, as shown on the left side in Figure 1e. It is found that the 800 nm thickness of the GaN film allows for the coexistence of resonance modes of different orders. For comparison, the reflectance spectrum calculated for the periodic structure with a 60 nm GaN film only exhibits the fundamental BIC mode within the emission band of GaN (right side in Figure 1e). The comparison between dispersion diagrams for the two cases is shown in Figure S2 (Supporting Information). Both dispersion curves exhibit flat curves around the Γ point, implying that the light is confined in the plane. The calculated electric near-field distributions of GaN BIC lasers for GaN films with a thickness of 800 and 60 nm are shown in Figure 1f, marked as A and B, respectively. Light is found to be confined without radiative loss in both structures. Furthermore, the resonance wavelengths of the BIC modes are found to shift with the gain thickness. That is, the resonance wavelength can be controlled by both the structure period and the GaN thickness. Consequently, the BIC resonance can be tuned to match the emission band of GaN without accurately controlling t_{GaN}, as shown in Figure S1b (Supporting Information), so that the original thickness of the GaN film can be utilized as prepared and no additional fabrication step such as etching is required. This renders the fabrication process completely free of etching steps.

2.2. Fabrication

The fabrication process of the GaN BIC laser is shown in Figure S3a (Supporting Information). First, an 800 nm GaN film is grown on a sapphire substrate using MOCVD. The film was characterized by ellipsometry, as shown in Figure S3b (Supporting Information). Then, the designed periodic structure is patterned on the GaN film by a one-step e-beam lithography. The ZEP520A e-beam resist is directly utilized as the material of the periodic structure supporting the BIC mode. This ZEP520A e-beam resist was selected to fabricate the periodic structure because it is known to possess nearly no absorption in the region of interest (see measured *n* and *k* values as well as absorption coefficient in reference[44]). Here, the effect of the resist slab thickness was investigated through simulations, as shown in Figure S3c,d (Supporting Information). It is concluded that varying the resist slab thickness from 20 to 100 nm has merely no effect on the formation of the BIC mode. In this work, the resist slabs of the periodic structure were fabricated with a thickness of 100 nm. Figure S3e (Supporting Information) shows the tilted-view scanning electron microscopy (SEM) image of the fabricated structure.

2.3. Characterization

The optical properties of the GaN BIC laser were characterized at room temperature. **Figure 2**a shows the emission spectra under different pump energy densities of the GaN BIC laser pumped by a 355 nm nanosecond laser. At a low pump energy density, the GaN BIC laser only shows a broad photoluminescence (PL) spectrum. As the pump energy increases, a single sharp lasing peak appears. Measured emission intensity and FWHM of the GaN BIC laser under different pump energy densities are plotted in Figure 2b. The measured threshold (P_{th}) for the GaN BIC laser is 16.0 mJ cm^{-2}, as determined by recording the nonlinear increase in the intensity and sharp decreases in the FWHM when the pump energy exceeds the threshold value. It is noted that a threshold of 1.3 mJ cm^{-2} is achieved when the period structure supporting the BIC mode is pumped by a femtosecond laser (Figure 2c). The difference in measured lasing thresholds when pumped by two different systems is believed to come from the efficiency difference between the fs-laser and the ns-laser excitation as the ultrafast femtosecond pumping should be more efficient to induce population inversion.[45] Figure 2d shows the optical images of the GaN laser when the pump energy density is below and above the lasing threshold. During the optical pumping process, light is found to propagate along the grating-vector direction (the *x*-axis, as defined in the lower-left corner of the figure), indicating light coupling to the line-and-space periodic structure. The high-resolution lasing spectrum plotted in Figure 2e exhibiting an FWHM of 0.10 nm is representative of the best-performing fabricated devices. This experimental result is among the smallest bandwidths reported for single-mode GaN lasing devices in the UV region (Table S1, Supporting Information),[29–31,33–34,37–40,46–52] giving a high $\lambda/\Delta\lambda$ (λ is the lasing wavelength and $\Delta\lambda$ the FWHM of the lasing linewidth.) of over 3700.

The far-field emission pattern of the GaN BIC laser taken in the objective-lens back focal plane is shown in Figure 2f. This pattern is collected with a numerical aperture (NA) of 0.45. The far-field pattern is composed of a dark band in the middle surrounded by two bright bands. The dark area in the middle of the image implies that the lasing comes from the BIC mode instead of the leaky mode.[20] The divergence angle of the two beams is observed to be slightly smaller than 1.5°, showing highly directional emission which is difficult to achieve for lasers based on Fabry-Perot cavities or microring/microdisk cavities supporting whispering-gallery-modes. Figure 2g shows the polarization of the GaN BIC laser emission. The lasing intensity is maximum when the transmission axis of the linear

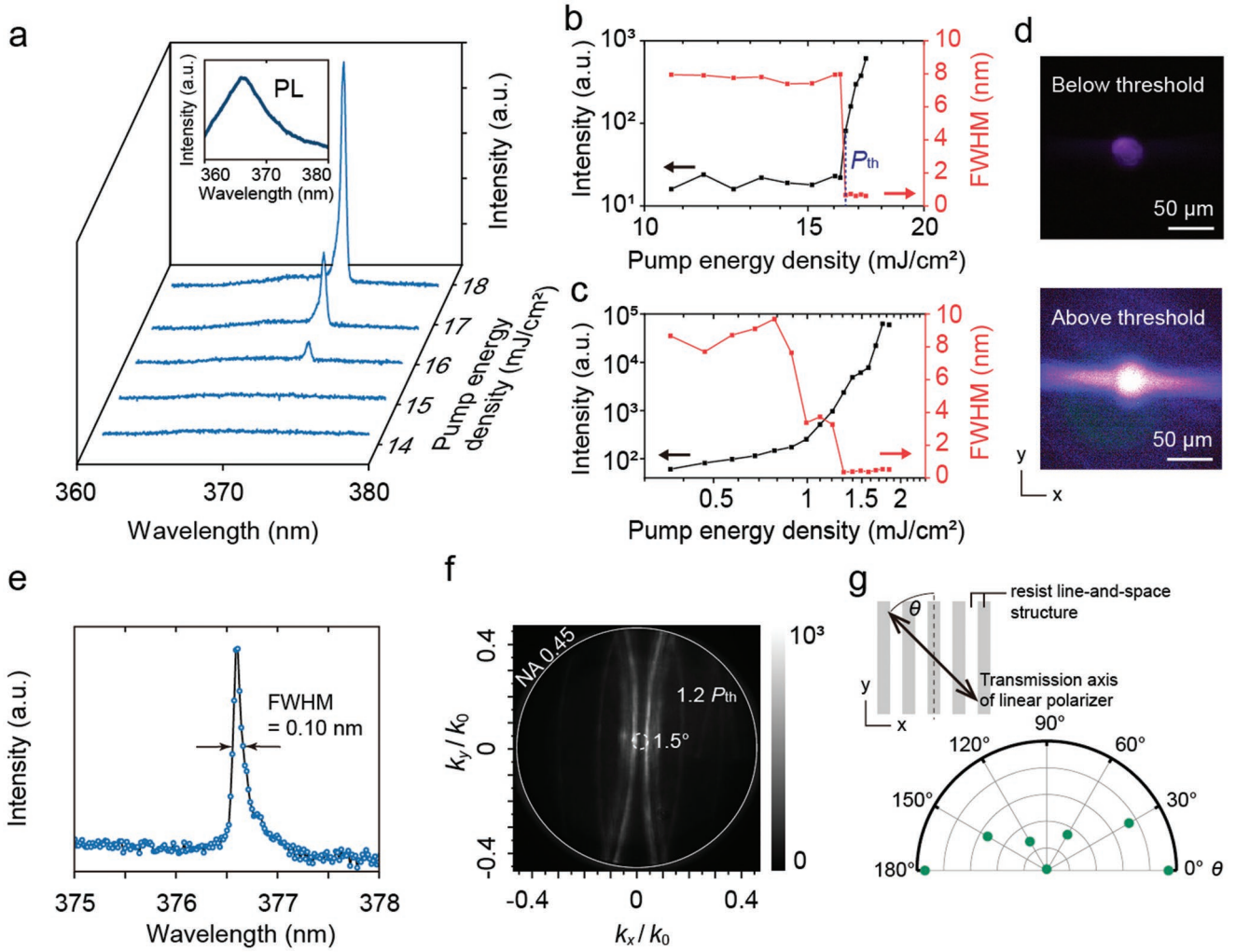

Figure 2. Lasing performance of the GaN BIC laser. a) Emission spectra of the GaN BIC laser under different pump energy densities. The inset is photoluminescence (PL) spectrum of the GaN BIC laser. b,c) The emission intensity and the full width at half-maximum (FWHM) as a function of pump energy density pumped by b) the 355 nm ns-laser and c) the 355 nm fs-laser. d) Optical images of the GaN BIC laser with the pump energy densities below and above the lasing threshold (P_{th}). e) The high-resolution spectrum of the single-mode lasing showing an FWHM of 0.10 nm. f) The far-field emission pattern collected at the back focal plane of the objective lens with a numerical aperture (NA) of 0.45. g) Measured lasing intensity under different polarizations indicated by θ, which indicates the angle between the slab direction and the transmission axis of the linear polarizer.

polarizer is parallel to the slab direction of the periodic structure ($\theta = 0°$ or 180°) and gradually becomes lower as the polarizer rotates toward the vertical direction ($\theta = 90°$). This shows that the emitted lasing of the GaN BIC laser is polarized along the slab direction corresponding to the *y*-axis.

2.4. Wavelength Control and Tunability

As the resonance wavelength of the BIC mode is controlled by the structure period Λ, the wavelength control of the GaN BIC laser can be realized by only varying the period on the same GaN film. Here, GaN BIC lasers with a period varying from 194.0 to 200.5 nm are fabricated and characterized. The measured spectra with normalized intensity are shown in **Figure 3**a, exhibiting a redshift in the lasing peak as the period increases. The experimental results agree well with the simulations of the reflectance spectra with different periods. Figure 3b shows that the wavelength of the BIC modes, along with the resonance bands in the spectra, shift toward larger wavelengths as the period increases. The dependence of the measured lasing wavelengths with the period is indicated as dark gray squares in Figure 3c, and the simulated resonance wavelengths with different periods are shown as red circles in the same figure for comparison. The observed variation of the lasing wavelength with the period is well reproduced by simulation. It is concluded that the control of the lasing wavelength from 371 to 377 nm with a 0.45 nm step was demonstrated.

Also, the temperature effect on lasing was studied by pumping the GaN BIC laser with a period of 200 nm. Emission spectra under different temperatures are plotted in **Figure 4**a. As the temperature increases from 273 to 383 K, the lasing peak is observed to redshift gradually from 375.8 to 380.1 nm. The operation of lasing at 383 K, which is among the highest

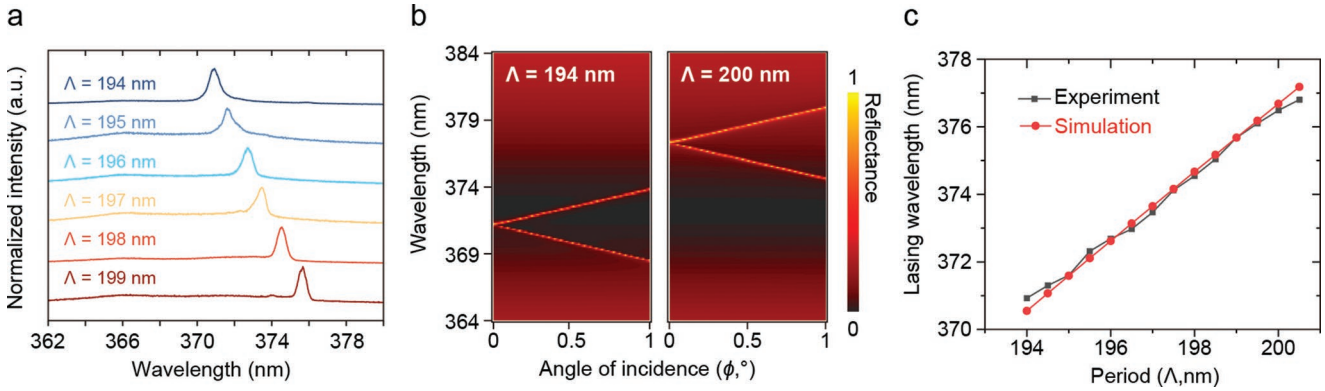

Figure 3. Lasing obtained with GaN BIC lasers with finely controlled period Λ. a) Emission spectra with normalized intensity obtained from GaN BIC lasers having different periods. b) Simulated reflectance spectra with structure periods of 194 and 200 nm. c) Experimental and simulated dependence of lasing wavelengths on the period.

operating temperatures for the reported single-mode GaN lasers (see Table S1, Supporting Information),[29–31,33–34,37–40,46–52] indicates the potential of the proposed BIC laser design for practical applications under relatively high-temperature environment. The shift can be attributed to the change in the refractive index of GaN near the emission band edge since simulations conducted with temperature-corrected refractive indices of GaN exhibit the same redshift trend with a similar slope, as seen in Figure 4b which gives the lasing wavelength dependence with the temperature obtained in experiments (dark gray squares) and simulations (red circles). The agreement shows that the wavelength tunability is achieved by varying the temperature. It is noted that the tunable range of lasing can be extended to approximately 380 nm due to the broadening and redshift of the emission band of GaN with increased temperature, as revealed by the PL spectra of Figure 4c. Also, an increase in the lasing threshold with temperature was observed in Figure 4d. This degradation of the lasing threshold is due to a lower gain

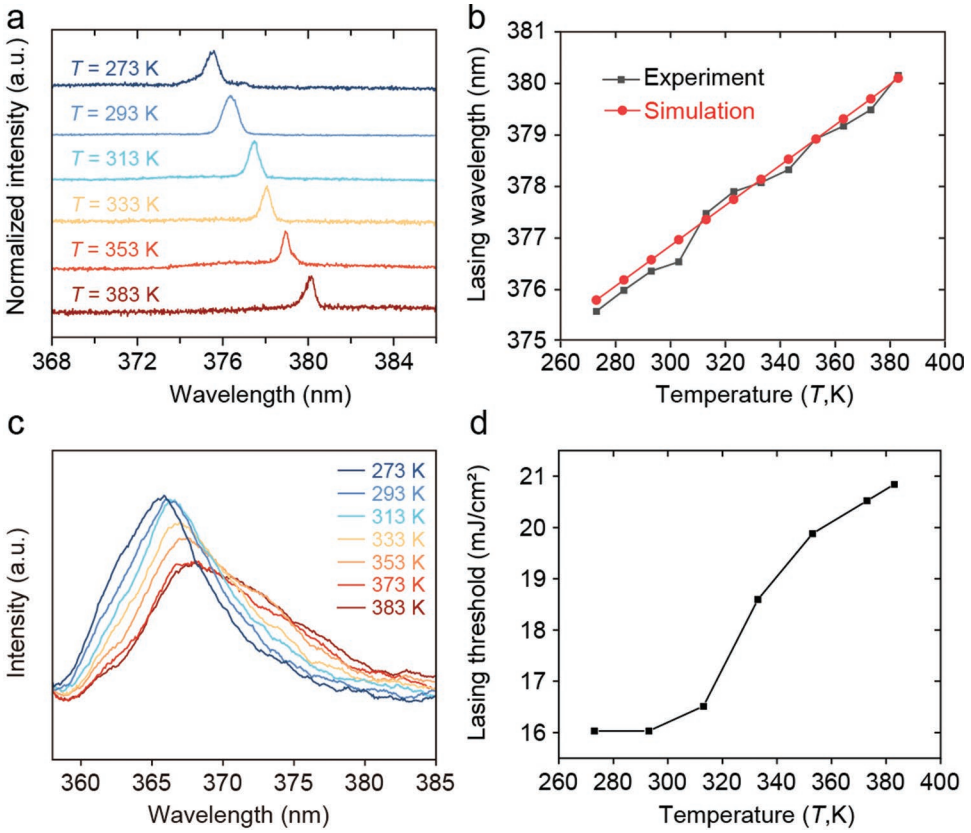

Figure 4. Effects of temperature (*T*) on lasing. a) Emission spectra of the 200-nm-period GaN BIC laser obtained under varying temperature from 273 to 383 K. b) Experimental and simulated dependences of the lasing wavelength with temperature. c) Measured photoluminescence (PL) spectra of the GaN film at different temperatures. d) Dependence of the measured lasing threshold with temperature.

of GaN caused by the increase in the nonradiative recombination rate with temperature.[33]

2.5. Effects of Material Absorption and Finite Structure Sizes on the Quasi-BIC Laser

Although ideal BIC modes can be utilized to achieve resonances with Q near infinity, a real periodic structure supporting the BIC mode, however, only reaches finite Q due to fabrication imperfection, material absorption, and finite sizes of the structure. The effect of the absorption of the resist slabs was investigated through simulations and plotted in Figure S4 (Supporting Information). It is found that Q drops to a finite number when the resist slabs possess a small material absorption k.

Next, the effect of the finite periodic structure size on lasing thresholds, which is an important issue for laser devices, was investigated experimentally by fabricating a set of samples composed of periodic structures of different sizes on the same GaN film. The periods of these structures are fixed at the same value. The fabricated patterns differ in the number of resist slabs (N) and corresponding areas. Experimental results are plotted in **Figure 5**a, where the lasing threshold in terms of energy density is found to increase from 16 to 24.5 mJ cm^{-2} as the size of the laser shrinks from 2304 to 64 μm^2. The threshold difference can be attributed to the drop of Q for the finite periodic structure supporting quasi-BIC mode when N decreases. In this work, the small lasing structure was demonstrated with a side length of 8 μm (N = 40) (Table S2, Supporting Information).[14–18,20–24,42,53] It is noted that the size is also small compared to the reported GaN-based VCSELs.[39,40] The optical feedback mechanism under different N values is investigated by simulations, as shown in Figures S5 and S6 (Supporting Information). For a structure with a large N, the field distribution shows the typical standing wave behavior along the x- and z- directions, providing optical feedback for lasing. For a structure with a small N, the confinement in the x-direction becomes weaker, but the oscillations in the z-direction can still provide feedback for light amplification. That is, both modes contribute to the lasing emission. Based on the different sizes of the fabricated lasers, the lasing thresholds are calculated in terms of the total pump energy, that is, the energy densities multiplied by the effective pump area. (Here, the pump beam size in the experiment is 48 μm in diameter. The effective pump area refers to the laser area that is under pumping. That is, the effective pump area for a laser is equivalent to the laser area if the pump beam is completely within the laser.) This normalized relation between the total Pump energy and the laser area is plotted in Figure 5b, showing a linear relationship between the two parameters. The threshold of the smallest GaN BIC laser is found to be 15.7 nJ.

3. Conclusion

Based on the concept of optical BIC, we demonstrate a BIC-based laser in the UV region consisting of a 1D resist line-and-space periodic structure on a GaN film. The laser structure is fabricated without etching steps thus preserving the quality of the GaN gain medium. Lasing linewidth as small as 0.10 nm (FWHM) was achieved thus providing a linewidth among the smallest reported for single-mode GaN-based UV micro-/nanolasers. The recorded far-field emission patterns and the polarization states indicate that an out-of-plane lasing emission with linear polarization is achieved. Moreover, the wavelength control of the GaN BIC lasers over the range from 371 to 380 nm was demonstrated by varying the structure period and the temperature. Finally, the dependence of the lasing threshold on the size of the GaN BIC structure showed that lasing can still be obtained for a structure size of 8 μm. This work provides a means to design tunable micro-/nanolasers with low-divergence and out-of-plane UV emissions.

4. Experimental Section

Simulation: The far-field reflectance spectra were calculated using the rigorous coupled-wave analysis (RCWA, RSoft Design Group, USA). The electric field distributions of the modes were computed using eigenfrequency studies (COMSOL Multiphysics, COMSOL, Inc., USA).

Laser Fabrication: The GaN film was synthesized using MOCVD and characterized by ellipsometry (M-2000U, J.A. Woollam, USA). The resist line-and-space periodic structures were fabricated on a 10 × 10 mm^2 GaN film by e-beam lithography. First, the OAP solution (hexamethyldisilazane, HMDS) was spin-coated (3000 rpm for 30 s) onto the GaN film and baked at 110 °C for 1 min. Second, a 100 nm e-beam resist layer (ZEP520A, diluted with anisole (1:1)) was spin-coated

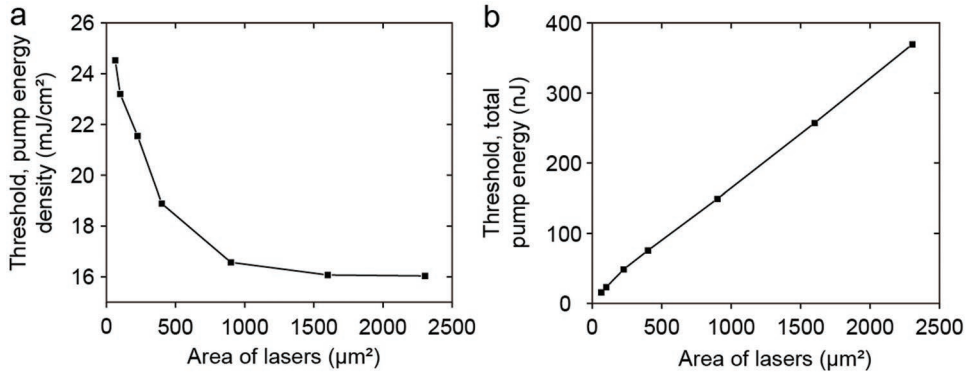

Figure 5. The effect of the size of the GaN BIC laser on the lasing threshold. The lasing threshold of GaN BIC lasers with different sizes is shown in terms of a) pump energy density and b) total pump energy.

(6000 rpm for 2 min) onto the film and baked at 180 °C for 3 min. Third, an Espacer layer (300Z, Showa Denko, Japan) was spin-coated (4000 rpm for 60 s) onto the resist layer and baked at 110 °C for 10 min. Then, the designed patterns were written with the e-beam lithography system (F7000S-VD02, Advantest, Japan). After that, the sample was rinsed with water for 60 s, developed in ZED-N50 (n-amyl acetate) for 30 s, and rinsed with MIBK (methyl isobutyl ketone) for 30 s. After development, the sample was dried in ambient air.

Optical Measurement: The experimental optical properties of the fabricated lasers were obtained by pumping the samples with a 0.6 ns laser pulse at 355 nm with a repetition rate of 1 kHz (picolo AOT 1-MOPA, InnoLas Laser, Germany) except for the emission properties shown in Figure 2d, which was obtained with a 250 fs laser pulse at 355 nm with a repetition rate of 75 kHz (Orpheus-HP, Light Conversion, Lithuania). The homemade experimental setup for lasing characterization is shown in Figure S7 (Supporting Information). The pump light was focused by an objective lens with a magnification of 20 times and a numerical aperture of 0.45. The excited emission was collected and analyzed with a spectrometer (SpectraPro HRS-500, Princeton Instruments, USA). The optical images and the back focal plane images are collected with two CCD cameras (CS505CU, Thorlabs, Inc., USA and CS165MU/M, Thorlabs, Inc., USA), respectively. The temperature-dependent lasing properties were characterized on a temperature-controlled microscope stage (10084L, Linkam Scientific Instruments, UK).

Supporting Information

Supporting Information is available from the Wiley Online Library or from the author.

Acknowledgements

M.-H.C. and D.X. contributed equally to this work. This work was supported by JSPS KAKENHI (JP20H02197, JP21H01383, JP21J11825, and JP20F40045) and the Ministry of Science and Technology, Taiwan (110-2221-E-239-026-MY3). This work was supported by "Advanced Research Infrastructure for Materials and Nanotechnology in Japan (ARIM)" of the Ministry of Education, Culture, Sports, Science and Technology (MEXT). Proposal Number JPMXP1222UT1026. The authors would like to extend their grateful appreciation to Professor Kuniaki Konishi and Professor Junji Yumoto from the School of Science, The University of Tokyo for their important technical support. M.-H.C. acknowledges the fellowship from WINGS-QSTEP.

Conflict of Interest

The authors declare no conflict of interest.

Data Availability Statement

The data that support the findings of this study are available from the corresponding author upon reasonable request.

Keywords

bound states in the continuum, GaN lasers, surface-emitting lasers, ultraviolet lasers

Received: August 16, 2022
Revised: November 29, 2022
Published online:

[1] C. W. Hsu, B. Zhen, A. D. Stone, J. D. Joannopoulos, M. Soljačić, *Nat. Rev. Mater.* **2016**, *1*, 16048.
[2] D. P. Bour, N. W. Carlson, G. A. Evans, S. K. Liew, J. B. Kirk, W. F. Reichert, *J. Appl. Phys.* **1991**, *70*, 4687.
[3] R. Kazarinov, C. Henry, *IEEE J. Quantum Electron.* **1985**, *21*, 144.
[4] Y. Plotnik, O. Peleg, F. Dreisow, M. Heinrich, S. Nolte, A. Szameit, M. Segev, *Phys. Rev. Lett.* **2011**, *107*, 183901.
[5] C. W. Hsu, B. Zhen, J. Lee, S. L. Chua, S. G. Johnson, J. D. Joannopoulos, M. Soljacic, *Nature* **2013**, *499*, 188.
[6] R. K. C. Henry, R. Logan, R. Yen, *IEEE J. Quantum Electron.* **1985**, *21*, 151.
[7] S. I. Azzam, V. M. Shalaev, A. Boltasseva, A. V. Kildishev, *Phys. Rev. Lett.* **2018**, *121*, 253901.
[8] Y. Liang, K. Koshelev, F. Zhang, H. Lin, S. Lin, J. Wu, B. Jia, Y. Kivshar, *Nano Lett.* **2020**, *20*, 6351.
[9] F. Yesilkoy, E. R. Arvelo, Y. Jahani, M. Liu, A. Tittl, V. Cevher, Y. Kivshar, H. Altug, *Nat. Photonics* **2019**, *13*, 390.
[10] L. Xu, K. Zangeneh Kamali, L. Huang, M. Rahmani, A. Smirnov, R. Camacho-Morales, Y. Ma, G. Zhang, M. Woolley, D. Neshev, A. E. Miroshnichenko, *Adv. Sci.* **2019**, *6*, 1802119.
[11] I. S. Sinev, K. Koshelev, Z. Liu, A. Rudenko, K. Ladutenko, A. Shcherbakov, Z. Sadrieva, M. Baranov, T. Itina, J. Liu, A. A. Bogdanov, Y. Kivshar, *Nano Lett.* **2021**, *21*, 8848.
[12] Z. Yu, X. Xi, J. Ma, H. K. Tsang, C.-L. Zou, X. Sun, *Optica* **2019**, *9*, 683.
[13] Z. Yu, Y. Tong, H. K. Tsang, X. Sun, *Nat. Commun.* **2020**, *11*, 2602.
[14] M. S. Hwang, H. C. Lee, K. H. Kim, K. Y. Jeong, S. H. Kwon, K. Koshelev, Y. Kivshar, H. G. Park, *Nat. Commun.* **2021**, *12*, 4135.
[15] A. Kodigala, T. Lepetit, Q. Gu, B. Bahari, Y. Fainman, B. Kante, *Nature* **2017**, *541*, 196.
[16] S. Mohamed, J. Wang, H. Rekola, J. Heikkinen, B. Asamoah, L. Shi, T. K. Hakala, *Laser Photonics Rev.* **2022**, *2*, 2100574.
[17] S. T. Ha, Y. H. Fu, N. K. Emani, Z. Pan, R. M. Bakker, R. Paniagua-Dominguez, A. I. Kuznetsov, *Nat. Nanotechnol.* **2018**, *13*, 1042.
[18] C. Z. Can Huang, S. Xiao, Y. Wang, Y. Fan, Y. Liu, N. Zhang, G. Qu, H. Ji, J. Han, L.i Ge, Y. Kivshar, Q. Song, *Science* **2020**, *367*, 1018.
[19] V. Mylnikov, S. T. Ha, Z. Pan, V. Valuckas, R. Paniagua-Dominguez, H. V. Demir, A. I. Kuznetsov, *ACS Nano* **2020**, *14*, 7338.
[20] Y. Wang, Y. Fan, X. Zhang, H. Tang, Q. Song, J. Han, S. Xiao, *ACS Nano* **2021**, *15*, 7386.
[21] S. I. Azzam, K. Chaudhuri, A. Lagutchev, Z. Jacob, Y. L. Kim, V. M. Shalaev, A. Boltasseva, A. V. Kildishev, *Laser Photonics Rev.* **2021**, *15*.
[22] M. Wu, L. Ding, R. P. Sabatini, L. K. Sagar, G. Bappi, R. Paniagua-Dominguez, E. H. Sargent, A. I. Kuznetsov, *Nano Lett.* **2021**, *21*, 9754.
[23] J. H. Yang, Z. T. Huang, D. N. Maksimov, P. S. Pankin, I. V. Timofeev, K. B. Hong, H. Li, J. W. Chen, C. Y. Hsu, Y. Y. Liu, T. C. Lu, T. R. Lin, C. S. Yang, K. P. Chen, *Laser Photonics Rev.* **2021**, *15*, 2100118.
[24] M. Wu, S. T. Ha, S. Shendre, E. G. Durmusoglu, W. K. Koh, D. R. Abujetas, J. A. Sanchez-Gil, R. Paniagua-Dominguez, H. V. Demir, A. I. Kuznetsov, *Nano Lett.* **2020**, *20*, 6005.
[25] I. G. M. Leszczynski, M. Bockowski, *J. Cryst. Growth* **1993**, *126*, 601.
[26] M. Imanishi, T. Yoshida, T. Kitamura, K. Murakami, M. Imade, M. Yoshimura, M. Shibata, Y. Tsusaka, J. Matsui, Y. Mori, *Cryst. Growth Des.* **2017**, *17*, 3806.
[27] R. Dingle, K. L. Shaklee, R. F. Leheny, R. B. Zetterstrom, *Appl. Phys. Lett.* **1971**, *19*, 5.
[28] X. H. Yang, T. J. Schmidt, W. Shan, J. J. Song, B. Goldenberg, *Appl. Phys. Lett.* **1995**, *66*, 1.
[29] J. C. Johnson, H. J. Choi, K. P. Knutsen, R. D. Schaller, P. Yang, R. J. Saykally, *Nat. Mater.* **2002**, *1*, 106.

[30] H. Xu, J. B. Wright, T.-S. Luk, J. J. Figiel, K. Cross, L. F. Lester, G. Balakrishnan, G. T. Wang, I. Brener, Q. Li, *Appl. Phys. Lett.* **2012**, *101*, 113106.
[31] Q. Zhang, G. Li, X. Liu, F. Qian, Y. Li, T. C. Sum, C. M. Lieber, Q. Xiong, *Nat. Commun.* **2014**, *5*, 4953.
[32] H. Liu, H. Zhang, L. Dong, Y. Zhang, C. Pan, *Nanotechnology* **2016**, *27*, 355201.
[33] S. Sergent, B. Damilano, S. Vézian, S. Chenot, T. Tsuchizawa, M. Notomi, *Appl. Phys. Lett.* **2020**, *116*, 223101.
[34] G. Zhu, J. Li, J. Li, J. Guo, J. Dai, C. Xu, Y. Wang, *Opt. Lett.* **2018**, *43*, 647.
[35] G. Zhu, J. Li, N. Zhang, X. Li, J. Dai, Q. Cui, Q. Song, C. Xu, Y. Wang, *Sci. Rep.* **2020**, *10*, 253.
[36] G. He, F. Qin, C. Xu, C. Wang, Y. Xu, B. Cao, K. Xu, *J. Mater. Sci. Technol.* **2020**, *53*, 140.
[37] G. Zhu, S. He, J. Li, J. Yuan, F. Qin, J. Li, X. Li, Y. Wang, *Opt. Commun.* **2020**, *474*.
[38] F. F. Qin, G. Y. Zhu, J. B. Yang, L. Wei, Q. N. Cui, Y. J. Wang, *Nanoscale* **2022**, *14*, 1921.
[39] K.-J. Chen, W.-H. Hsu, W.-C. Liao, S.-W. Liao, M.-H. Shih, H.-C. Kuo, *IEEE J. Sel. Top. Quantum Electron.* **2015**, *21*, 475.
[40] J.-Y. Zhang, L.-E. Cai, B.-P. Zhang, S.-Q. Li, F. Lin, J.-Z. Shang, D.-X. Wang, K.-C. Lin, J.-Z. Yu, Q.-M. Wang, *J. Lightwave Technol.* **2009**, *27*, 55.
[41] C. R. Webster, L. Wöste, R. N. Zare, *Opt. Commun.* **1980**, *35*, 435.
[42] Y. W. Wanhua Zheng, M. Wang, T. Fu, X. Zhou, X. Wang, W. Liu, J. Fan, A. Qi, G. Li, Y. Kivshar, *Preprint (Version 1) available at Research Square* **2022**, https://doi.org/10.21203/rs.3.rs-1510605/v1.
[43] S. D. Krasikov, A. A. Bogdanov, I. V. Iorsh, *Phys. Rev. B* **2018**, *97*, 224309.
[44] D. K. Brown, *J. Vac. Sci. Technol., B: Microelectron. Nanometer Struct.–Process., Meas., Phenom.* **2007**, *25*, 2447.
[45] T. M. Drane, H. Bach, M. Shapiro, V. Milner, *Biomed. Opt. Express* **2015**, *6*, 1885.
[46] Q. Li, J. B. Wright, W. W. Chow, T. S. Luk, I. Brener, L. F. Lester, G. T. Wang, *Opt. Express* **2012**, *20*, 17873.
[47] J. Heo, S. Jahangir, B. Xiao, P. Bhattacharya, *Nano Lett.* **2013**, *13*, 2376.
[48] C. Tessarek, R. Röder, T. Michalsky, S. Geburt, H. Franke, R. Schmidt-Grund, M. Heilmann, B. Hoffmann, C. Ronning, M. Grundmann, S. Christiansen, *ACS Photonics* **2014**, *1*, 990.
[49] W.-C. Liao, S.-W. Liao, K.-J. Chen, Y.-H. Hsiao, S.-W. Chang, H.-C. Kuo, M.-H. Shih, *Sci. Rep.* **2016**, *6*, 26578.
[50] H. Chen, J. Li, G. Yu, H. Zong, R. Lang, M. Lei, S. Li, M. S. A. Khan, Y. Yang, T. Wei, H. Liao, L. Meng, P. Wen, X. Hu, *Opt. Express* **2022**, *30*, 16794.
[51] T. Kouno, K. Kishino, T. Suzuki, M. Sakai, *IEEE Photonics J.* **2010**, *2*, 1027.
[52] P. Ghosh, D. Yu, T. Hu, J. Liang, Z. Chen, L. Yingkai, M. Huang, *J. Mater. Sci.* **2019**, *54*, 8472.
[53] R. Heilmann, G. Salerno, J. Cuerda, T. K. Hakala, P. Torma, *ACS Photonics* **2022**, *9*, 224.